

# Source-free exchange-correlation magnetic fields in density functional theory

S. Sharma<sup>1,\*</sup>, E. K. U. Gross<sup>1</sup>, A. Sanna<sup>1</sup>, and J. K. Dewhurst<sup>1</sup>

<sup>1</sup>*Max-Planck Institut für Mikrostruktur Physics,  
Weinberg 2, D-06120 Halle, Germany*

(Dated: April 18, 2017)

## Abstract

Spin-dependent exchange-correlation energy functionals in use today depend on the charge density and the magnetization density:  $E_{xc}[\rho, \mathbf{m}]$ . However, it is also correct to define the functional in terms of the curl of  $\mathbf{m}$  for physical external fields:  $E_{xc}[\rho, \nabla \times \mathbf{m}]$ . The exchange-correlation magnetic field,  $\mathbf{B}_{xc}$ , then becomes source-free. We study this variation of the theory by uniquely removing the source term from local and generalized gradient approximations to the functional. By doing so, the total Kohn-Sham moments are improved for a wide range of materials for both functionals. Significantly, the moments for the pnictides are now in good agreement with experiment. We also predict dramatic differences in the spatial geometry of  $\mathbf{B}_{xc}$  for the pnictides. Our source-free method is simple to implement in all existing density functional theory codes.

PACS numbers:

Density functional theory (DFT)[1, 2] has proven enormously successful for calculating the electronic structure of both molecules and solids. Lattice structures, phonon spectra and many other properties are now routinely calculated. Magnetism presents more of a mixed picture. Simple magnets, such as elemental solids (Fe, Co and Ni), are well-described by the local spin density approximation (LSDA)[3] or the generalized gradient approximations (GGA)[4], at least as far as total moments are concerned. However, both LSDA and GGA perform poorly for the iron pnictide and related materials[5–8] for which they greatly over-estimate the moments by factors of two or more (see Fig. 1). This has been an impediment to investigating the microscopic magnetic structure[9–13], related response functions[14] and superconductivity [15–17] of these materials with density functional methods.

Most approximate spin-dependent exchange-correlation energy functionals,  $E_{\text{xc}}[\rho, \mathbf{m}]$ , use the density and magnetization as their arguments[18–21]. This form is dictated by the many-body Hamiltonian used originally in the context of spin DFT (SDFT) by von Barth and Hedin[18]:

$$\hat{H} = \sum_{i=1} -\frac{1}{2}\nabla_i^2 + V_{\text{ext}}(\mathbf{r}_i) + \vec{\sigma} \cdot \mathbf{B}_{\text{ext}}(\mathbf{r}_i) + \frac{1}{2} \sum_{j \neq i} \frac{1}{|\mathbf{r}_i - \mathbf{r}_j|}, \quad (1)$$

where  $V_{\text{ext}}$  and  $\mathbf{B}_{\text{ext}}$  are the external scalar potential and magnetic fields, respectively; and the sum runs to the number of particles. The external magnetic field was assumed to be an unconstrained vector field in the original formulation of SDFT. Physical magnetic fields are not unconstrained but rather the curl of a vector potential, i.e.  $\mathbf{B}_{\text{ext}} = \nabla \times \mathbf{A}_{\text{ext}}$ . With this constraint it is possible to demonstrate (see [22, 23] and Appendix) that the exchange-correlation functional can be chosen to depend on the spin current  $\nabla \times \mathbf{m}(\mathbf{r})$  instead of  $\mathbf{m}(\mathbf{r})$ :  $\tilde{E}_{\text{xc}}[\rho, \nabla \times \mathbf{m}]$ .

An immediate consequence of this is that the functional derivative of  $\tilde{E}_{\text{xc}}[\rho, \nabla \times \mathbf{m}]$  with respect to  $\mathbf{m}(\mathbf{r})$  is of the form  $\tilde{\mathbf{B}}_{\text{xc}}(\mathbf{r}) \equiv \delta \tilde{E}_{\text{xc}} / \delta \mathbf{m}(\mathbf{r}) = \nabla \times \mathbf{A}_{\text{xc}}(\mathbf{r})$  which implies  $\nabla \cdot \mathbf{B}_{\text{xc}}(\mathbf{r}) = 0$ . In other words, the exchange-correlation magnetic field is *source-free*.

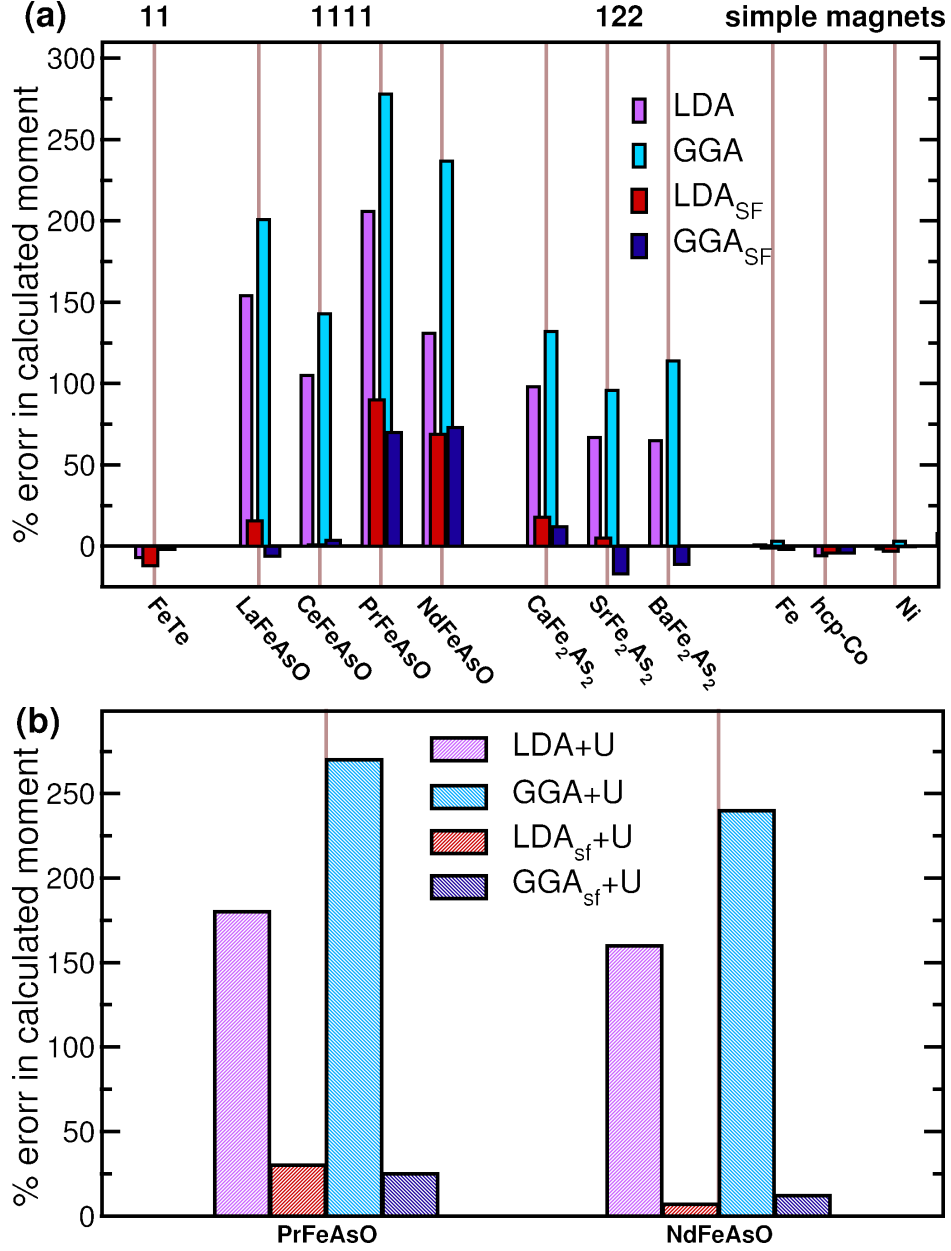


FIG. 1: Percentage deviation of the calculated magnetic moment from experimental data for 11, 1111, 122 pnictides as well as elemental solids. (a) Results calculated using LSDA (pink), GGA (cyan), and their source-free counterparts LSDA<sub>SF</sub> (red) and GGA<sub>SF</sub> (blue) (b) same as (a) but by adding an on-site Coulomb repulsion  $U$  on the  $f$ -states. Root-mean-square-percentage errors are LSDA: 90.2%, GGA: 143%, LSDA<sub>SF</sub>: 34%, GGA<sub>SF</sub>: 31%, LSDA<sub>SF</sub>+ $U$ : 16%, GGA<sub>SF</sub>+ $U$ : 11%.

An essential aspect of this version of SDFT, and one which has been seemingly overlooked in the past, is that the Kohn-Sham magnetization  $\mathbf{m}(\mathbf{r})$  obtained from the exact  $\tilde{\mathbf{B}}_{\text{xc}}$  is *not* itself exact, but rather only its curl is. The difference between the two is a curl-free

function which is therefore the gradient of some scalar function:  $\nabla f(\mathbf{r})$ . Thus one loses some information about the magnetization by using the source-free theory but not, as it turns out, the total moment. For finite systems, the total moment obtained from the Kohn-Sham magnetization using  $\tilde{\mathbf{B}}_{\text{xc}}$  is also exact because the integral of  $\nabla f(\mathbf{r})$  over all space is zero. This is not true for periodic boundary conditions, however. In this case, the functional domain has to be augmented with the total moment vector  $\mathbf{M}$ , thus  $\tilde{E}_{\text{xc}} \equiv \tilde{E}_{\text{xc}}[\rho, \nabla \times \mathbf{m}, \mathbf{M}]$ . This is analogous to the macroscopic polarization required as an extra variable in presence of an external electric field applied to a solid[24]. The variable conjugate to  $\mathbf{M}$  now has to be included in the calculation; this variable is clearly a constant magnetic field and corresponds to an  $\mathbf{A}_{\text{ext}}$  which diverges at large distance.

Functionals in common use, such as LSDA and GGA, are not, in general, source-free. This is confirmed simply by computing  $\nabla \cdot \mathbf{B}_{\text{xc}}(\mathbf{r})$  for a magnetic material. One may therefore reasonably ask: how can LSDA or GGA be modified so that they do have this property, i.e. how can any approximate  $\mathbf{B}_{\text{xc}}$  be made source-free? We appeal to Helmholtz's theorem which states that any vector field on a domain in  $\mathbb{R}^3$ , which is twice differentiable can be decomposed into a curl-free component and a source-free component. This decomposition is unique for given boundary conditions. Thus let  $\phi$  be the solution to Poisson's equation (in atomic units)

$$\nabla^2 \phi(\mathbf{r}) = -4\pi \nabla \cdot \mathbf{B}_{\text{xc}}(\mathbf{r}) \quad (2)$$

and define

$$\tilde{\mathbf{B}}_{\text{xc}}(\mathbf{r}) \equiv \mathbf{B}_{\text{xc}}(\mathbf{r}) + \frac{1}{4\pi} \nabla \phi(\mathbf{r}) \quad (3)$$

then  $\nabla \cdot \tilde{\mathbf{B}}_{\text{xc}}(\mathbf{r}) = 0$ , i.e.  $\tilde{\mathbf{B}}_{\text{xc}}$  is source-free. It is important to note that that the scalar part of the potential,  $V_{\text{xc}}(\mathbf{r})$ , is not directly affected by this procedure. This modified functional has certain intrinsic properties: (a) it is still correct for homogeneous electron gas (HEG) because  $\mathbf{B}_{\text{xc}}^{\text{HEG}}$  is a constant implying that  $\nabla \cdot \mathbf{B}_{\text{xc}}(\mathbf{r}) = 0$  and therefore this modification has no effect, (b) since  $\tilde{\mathbf{B}}_{\text{xc}}$  is obtained by solving Poisson's equation, the functional is intrinsically non-local, in other words, the field at  $\mathbf{r}$  depends on the magnetization everywhere, (c)  $\tilde{\mathbf{B}}_{\text{xc}}$  is necessarily non-collinear, (d)  $\mathbf{m}(\mathbf{r}) \times \tilde{\mathbf{B}}_{\text{xc}}(\mathbf{r})$  is non-zero and hence will contribute to spin-dynamics even in the absence of the external field[25], (e)  $\tilde{\mathbf{B}}_{\text{xc}}$  is not, in general, the functional derivative of an energy functional (see Appendix), (f) the procedure is simple to implement

in any code since all codes have a Poisson equation solver, and (g) very little computational effort is needed for the modification.

We perform an additional modification of the functional which effectively enhances the spin splitting. It comprises of a simple scaling of the input magnetization  $E_{xc}[\rho, \mathbf{m}] \rightarrow E_{xc}[\rho, s\mathbf{m}]$  and then a further scaling of the resultant magnetic field  $\mathbf{B}_{xc} \rightarrow s\mathbf{B}_{xc}$  in order to keep the functional variational with respect to  $\mathbf{m}$ . This scaling is reminiscent of that performed by Ortenzi *et al.*[26]. The scaling factor  $s$  is chosen empirically and we find that  $s = 1.12$  and  $s = 1.14$  are good choices for LSDA and GGA respectively, for a diverse set of materials. We note that this factor, though empirical, is not a material-dependent parameter.

In the present work we apply this procedure to LSDA and GGA: first we enhance the strength of the exchange splitting and then modify the functional in a unique way to become source-free. These new source-free functionals have the effect that: (a) the good moments of LSDA for elemental solids are retained, (b) the large overestimation of pnictide moments is cured, and (c) the GGA now yields better results than LSDA for both classes of materials. These results are illustrated in Fig. 1, where we show percentage errors for both common and pnictide materials, with both LSDA and GGA and their source-free counterparts. Our implementation is publicly available in the Elk Code[27] and so can be applied to many more such materials.

The percentage deviation in the magnetic moment from experiment are presented in Fig. 1(a). We note that the magnetic moments calculated using LSDA or GGA for simple magnets (Fe, Co and Ni) are already in very good agreement with experiment with maximum deviation of 8%. This is in contrast the moments for pnictides which deviate strongly from experiment with a maximum error of 278%. The moments calculated using source-free LSDA and GGA are also presented in Fig. 1(a) and for simple magnets they are of the same quality as that of the unmodified functionals. The fact that the integrated moments are the same does not necessarily imply that the magnetization densities are similar at each point in space. However, we find that for the simple magnets the two densities are fairly close at each point in space. In the case of pnictides, the moments show dramatic improvement. At a first glance it appears that LSDA<sub>SF</sub>/GGA<sub>SF</sub> substantially reduces the Fe moment for all pnictides compared to the corresponding LSDA/GGA value. A closer inspection, however, reveals that this reduction is, as it should be, highly selective in that the moment in SrFe<sub>2</sub>As<sub>2</sub>

TABLE I: Magnetic moment (in  $\mu_B$ ) per Fe atom for pnictides and per magnetic atom for the rest of the materials. For pnictides the moment is known to be highly sensitive to the structural details and hence the references for experimental structural data are cited in the first column and for magnetic moment in the second column.

Material	Expt	LSDA	LSDA <sub>SF</sub>	GGA	GGA <sub>SF</sub>
LaFeAsO[28]	0.63[29]	1.60	0.73	1.92	0.59
LaFeAsO[30]		1.39	0.7	1.8	0.58
CeFeAsO[31]	0.8[32]	1.64	0.81	1.95	0.83
PrFeAsO[33]	0.5[34]	1.53	0.99	1.89	0.85
NdFeAsO[35]	0.54[36]	1.24	0.91	1.82	0.93
CaFe <sub>2</sub> As <sub>2</sub> [37]	0.8[38]	1.59	0.95	1.86	0.90
SrFe <sub>2</sub> As <sub>2</sub> [39]	0.94[40]	1.57	0.98	1.84	0.78
BaFe <sub>2</sub> As <sub>2</sub> [41]	0.87[42]	1.43	0.87	1.84	0.78
BaFe <sub>2</sub> As <sub>2</sub> [30]		1.38	0.73	1.67	0.59
FeTe[43]	2.25[44]	2.10	1.73	2.25	1.85
bcc-Fe	2.2	2.15	2.22	2.27	2.16
hcp-Co	1.7	1.63	1.60	1.67	1.61
Ni	0.65	0.64	0.63	0.67	0.65
Ni <sub>3</sub> Al	0.077	0.17	0.1225	0.1825	0.1725
ZrZn <sub>2</sub>	0.085	0.21	0.197	0.283	0.257

is reduced by  $\sim 30\%$  while on LaFeAsO by  $\sim 60\%$  compared to the LSDA/GGA results. The maximum deviation is now less than 25% for all materials with the exception of NdFeAsO and PrFeAsO (see Table I).

For NdFeAsO and PrFeAsO the source-free functionals provide a considerable improvement over unmodified LSDA or GGA, but the percentage deviation from experiment is still relatively large. We find the reason behind this to be the moment on the rare earth atoms. In these materials the moment of the rare-earth atom is known to be strongly coupled to the moment on the Fe atoms[36] and the rare earth moment is not accurately described by the source-free functional alone[46]. In order to treat these we use the well-established method[47] of applying an on-site Coulomb repulsion  $U$ . It is important to mention that  $U$

TABLE II: Magnetic moment (in  $\mu_B$ ) per atom. Calculations are performed using LSDA+ $U$ , GGA+ $U$ , LSDA<sub>SF</sub> +  $U$  and GGA<sub>SF</sub> +  $U$ . The values of  $U$  and  $J$  used for these calculations are given in Ref. 45.

Material	Expt	LSDA	GGA	LSDA <sub>SF</sub>	GGA <sub>SF</sub>
PrFeAsO	Fe: 0.5	1.40	1.9	0.65	0.63
	Pr: 0.87	0.30	0.30	0.81	0.83
NdFeAsO	Fe: 0.54	1.42	1.84	0.50	0.61
	Nd: 0.9	2.44	1.25	0.80	0.89

was applied only to the  $f$ -states of the rare-earth atom and chosen to reproduce the experimental moment of that atom only. Nevertheless, this substantially improves the moment on the Fe sites (see Table II). Like experiments we find the moment on rare-earths to be in-plane and oriented perpendicular to the moment on the Fe atoms. The effect of the source-free functional is particularly apparent in these cases since without it the correct moment on either atom cannot be obtained for any choice of  $U$ .

A material that also requires special attention is LaFeAsO, perhaps the most studied pnictide of all. Reported experimental values of the magnetic moment range from  $0.36\mu_B$ [48] to  $0.8\mu_B$ [49] making it difficult to know to what our theoretical results should be compared. Perhaps the best choice is with the more recent experimental value which lies in between these two extremes,  $0.63\mu_B$ [29]. This experiment was performed at low temperature (2K) which is closest to our theoretical ideal of zero temperature. Another reasonable choice would be  $0.8\mu_B$ [49] since, like our theoretical work, these experiments are performed on single crystals. In either case, our results with source-free functionals still show a maximum deviation of 25%.

Note that the two steps which comprise this method (i.e. scaling and making the functional source-free) must be performed in combination; each applied alone yields unreasonable results (see Table III in Appendix).

A means of summarizing the overall quality of results is the root-mean-square percentage error (RMSPE) which one expects to be reduced on improving the functional, by going, for example, from LSDA to the more sophisticated GGA. To the contrary, the value of RMSPE for LSDA is 90.2% and for GGA is 143%, i.e. the quality of results deteriorates

on improving the functional by adding gradients. These errors are greatly reduced to 34.3% with  $\text{LSDA}_{\text{SF}}$  and 30.6% with  $\text{GGA}_{\text{SF}}$ . Furthermore, once the  $\text{LSDA}_{\text{SF}} + U$  and  $\text{GGA}_{\text{SF}} + U$  results are considered the RMSPE are 16% for source-free LSDA and 11% for source-free GGA, indicating that removal of the source term results in  $\text{GGA}_{\text{SF}}$  performing better than  $\text{LSDA}_{\text{SF}}$ .

It is also appropriate to ask under which circumstances do these source-free functionals fail? For the class of materials which are well known to be close to quantum critical points and for which spin-fluctuations dominate the physics[50, 51], i.e.  $\text{Ni}_3\text{Al}$  and  $\text{ZnZr}_2$ , the functional fails in that percentage errors compared to experiments, despite being an improvement over LSDA/GGA, are still large. Another aspect where  $\text{LSDA}_{\text{SF}}$  and  $\text{GGA}_{\text{SF}}$  are deficient is the fact that they are potential functionals and not energy functionals. Thus one cannot compare the total energies of various structural and magnetic configurations. Hence in the present work we have used experimental crystal structures. However, PBE is well known to be excellent for structural optimization in most cases, including magnetic pnictides, with lattice parameters very close to experiments and small deviations in the position of As atom [12, 52–55]. Hence one could perform a full optimization using PBE followed by a calculation using  $\text{LSDA}_{\text{SF}}$  or  $\text{GGA}_{\text{SF}}$ . To test this we have performed such calculations for  $\text{BaFe}_2\text{As}_2$  and  $\text{LaFeAsO}$  and find that the moment obtained using LSDA and GGA are still highly over-estimated (maximum error of 180%), while the moments obtained using  $\text{LSDA}_{\text{SF}}$  and  $\text{GGA}_{\text{SF}}$  are again within 25% of experiment (see Table I).

It is enlightening to see how  $\mathbf{B}_{\text{xc}}$  of LSDA and GGA and their new source-free versions differ spatially. We plot this for the case of  $\text{BaFe}_2\text{As}_2$  in Fig. 2. The field lines for LSDA are unphysical in the sense that they begin and end at different points whereas the source-free field lines are always closed. This means that they have to follow more complicated paths in the crystal, a fact evident from Fig. 2.

To summarize: motivated by an exact property of spin current DFT, we removed the source term from the  $\mathbf{B}_{\text{xc}}$  of LSDA and GGA. The spin splitting was also enhanced by a simple scaling of the input magnetization and output field. The resulting functionals were found to produce moments which were in better agreement with experiment. This improvement was particularly pronounced for the pnictides where errors were reduced from 100-200% down to 25% or less. We hope that our findings will spur the development of exchange-correlation energy functionals whose resultant magnetic fields are manifestly



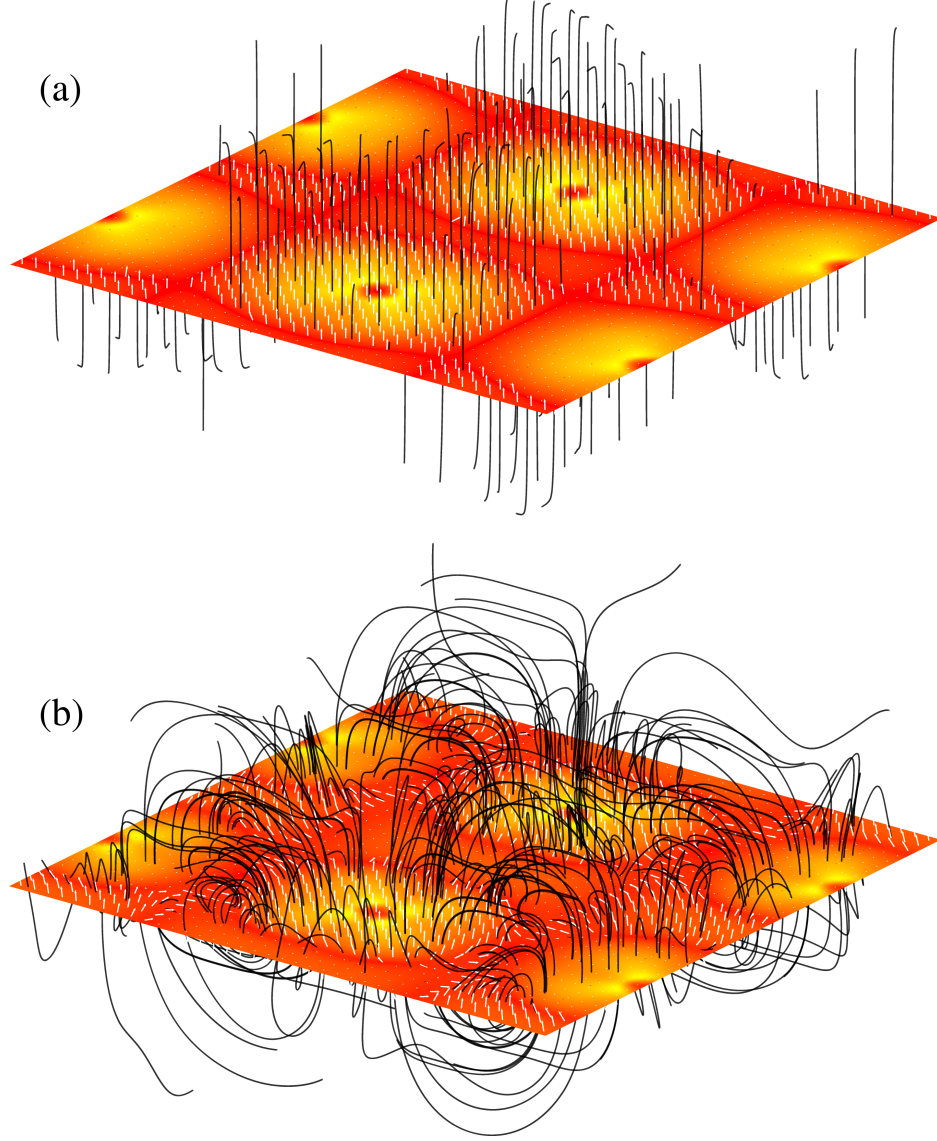


FIG. 2: The vector field  $\mathbf{B}_{xc}$  for  $\text{BaFe}_2\text{As}_2$ . Plot (a) is LSDA and plot (b) is source-free LSDA. The colored plane contains the Fe atoms and shows the magnitude of  $\mathbf{B}_{xc}$ , with the small white arrows indicating direction. The black field lines originate from a regular grid in the plane and follow the vector field.

source-free.

## ACKNOWLEDGMENTS

The authors would like to thank Kieron Burke and Carsten Ullrich for useful discussions.

## APPENDIX

### Showing $\mathbf{B}_{\text{xc}}$ can be chosen source-free

Let

$$E[V_{\text{ext}}, B_{\text{ext}}] = \min_{|\Psi\rangle} \langle \Psi | \hat{H} | \Psi \rangle, \quad (4)$$

where  $\hat{H}$  is given in Eq. (1) and the minimization is over all  $N$ -electron states  $|\Psi\rangle$ , be the total energy as a functional of the external potential and magnetic field. This can be written as a constrained minimization

$$E[V_{\text{ext}}, B_{\text{ext}}] = \min_{(\rho, \mathbf{m})} \min_{|\Psi\rangle \rightarrow (\rho, \mathbf{m})} \langle \Psi | \hat{H} | \Psi \rangle \quad (5)$$

$$= \min_{(\rho, \mathbf{m})} \left\{ \int d^3r V_{\text{ext}}(\mathbf{r}) \rho(\mathbf{r}) + \int d^3r \mathbf{B}_{\text{ext}}(\mathbf{r}) \cdot \mathbf{m}(\mathbf{r}) + F[\rho, \mathbf{m}] \right\}, \quad (6)$$

where

$$F[\rho, \mathbf{m}] \equiv \min_{|\Psi\rangle \rightarrow (\rho, \mathbf{m})} \langle \Psi | \hat{T} + \hat{V}_{\text{ee}} | \Psi \rangle \quad (7)$$

is a universal functional of density and magnetization;  $\hat{T}$  and  $\hat{V}_{\text{ee}}$  are the kinetic and electron-electron interaction parts of the Hamiltonian, respectively. Likewise, the non-interacting kinetic energy functional is defined as

$$T_s[\rho, \mathbf{m}] \equiv \min_{|\Psi\rangle \rightarrow (\rho, \mathbf{m})} \langle \Psi | \hat{T} | \Psi \rangle \quad (8)$$

from which is obtained the exchange-correlation energy functional  $E_{\text{xc}}[\rho, \mathbf{m}] \equiv F[\rho, \mathbf{m}] - T_s[\rho, \mathbf{m}] - E_{\text{H}}[\rho]$ , where  $E_{\text{H}}$  is the usual Hartree energy.

However, if we assume that the external magnetic field is physical, i.e.  $\mathbf{B}_{\text{ext}}(\mathbf{r}) = \nabla \times \mathbf{A}_{\text{ext}}(\mathbf{r})$ , and the magnetization tends to zero at large distance, then the classical energy of the external magnetic field can be written as

$$\int d^3r (\nabla \times \mathbf{A}_{\text{ext}}(\mathbf{r})) \cdot \mathbf{m}(\mathbf{r}) = \int d^3r \mathbf{A}_{\text{ext}}(\mathbf{r}) \cdot (\nabla \times \mathbf{m}(\mathbf{r})). \quad (9)$$

Thus we can define another universal functional  $\tilde{F}[\rho, \nabla \times \mathbf{m}]$  as

$$\tilde{F}[\rho, \nabla \times \mathbf{m}] \equiv \min_{|\Psi\rangle \rightarrow (\rho, \nabla \times \mathbf{m})} \langle \Psi | \hat{T} + \hat{V}_{\text{ee}} | \Psi \rangle, \quad (10)$$

with analogous functionals  $\tilde{T}[\rho, \nabla \times \mathbf{m}]$  and  $\tilde{E}_{\text{xc}}[\rho, \nabla \times \mathbf{m}]$ . On the space of densities obtained from physical external magnetic fields we have that  $E_{\text{xc}}[\rho, \mathbf{m}] = \tilde{E}_{\text{xc}}[\rho, \nabla \times \mathbf{m}]$ . This implies that the total energy obtained from both functionals is also the same for physical densities.

The equality of the functionals does not hold in general for densities obtained from external magnetic fields which have a source term. A consequence of this is that the unconstrained functional derivative of  $E_{\text{xc}}$  with respect to  $\mathbf{m}(\mathbf{r})$  is different for the two functionals, i.e.  $\mathbf{B}_{\text{xc}}(\mathbf{r}) \neq \tilde{\mathbf{B}}_{\text{xc}}(\mathbf{r})$  in general. The functional derivative of  $\tilde{E}_{\text{xc}}$  can be further evaluated as

$$\begin{aligned} \tilde{\mathbf{B}}_{\text{xc}}(\mathbf{r}) &\equiv \left. \frac{\delta \tilde{E}_{\text{xc}}[\rho, \nabla \times \mathbf{m}]}{\delta \mathbf{m}(\mathbf{r})} \right|_{\rho} \\ &= \int d^3 r' \frac{\delta (\nabla \times \mathbf{m}(\mathbf{r}'))}{\delta \mathbf{m}(\mathbf{r})} \left. \frac{\delta \tilde{E}_{\text{xc}}[\rho, \nabla \times \mathbf{m}]}{\delta (\nabla \times \mathbf{m}(\mathbf{r}'))} \right|_{\rho} \\ &= \nabla \times \mathbf{A}_{\text{xc}}(\mathbf{r}), \end{aligned} \tag{11}$$

proving that  $\tilde{\mathbf{B}}_{\text{xc}}$  is indeed source-free. We note that this derivation also holds for the case where  $\mathbf{A}_{\text{ext}}$  and  $\mathbf{m}$  are lattice-periodic. In this case, the surface term which had to be zero in order to derive Eq. (9), sums to zero over the faces of the periodic box.

### Showing $\tilde{\mathbf{B}}_{\text{xc}}$ is not the functional derivative of an $\tilde{E}_{\text{xc}}$

If  $\tilde{\mathbf{B}}_{\text{xc}}$  was indeed the functional derivative of a scalar, then it would follow that the second derivative would be symmetric in its arguments. It is simple to demonstrate that

$$\begin{aligned} \frac{\delta^2 \tilde{E}_{\text{xc}}}{\delta \mathbf{m}(\mathbf{r}) \delta \mathbf{m}(\mathbf{r}')} &\equiv \tilde{f}_{\text{xc}}(\mathbf{r}, \mathbf{r}') \\ &= f_{\text{xc}}(\mathbf{r}, \mathbf{r}') + \int d^3 r'' M(\mathbf{r}, \mathbf{r}'') f_{\text{xc}}(\mathbf{r}'', \mathbf{r}'), \end{aligned}$$

where

$$M(\mathbf{r}, \mathbf{r}'') = \nabla_r \otimes \nabla_r \frac{1}{|\mathbf{r} - \mathbf{r}''|}$$

and  $f_{\text{xc}}(\mathbf{r}, \mathbf{r}')$  is a  $3 \times 3$  matrix. If  $M$  had been a Dirac delta function then  $\tilde{f}_{\text{xc}}$  would be symmetric in its arguments. This is not the case though and hence  $\tilde{\mathbf{B}}_{\text{xc}}$  is not the functional derivative of an  $\tilde{E}_{\text{xc}}$ . However,  $M$  is highly localized in  $|\mathbf{r} - \mathbf{r}''|$ .

## Computational details

The full potential linearized augmented plane wave (LAPW) method implemented within the Elk code[27] is used in the present work. All calculations are performed in the presence of the spin-orbit coupling. To obtain the Pauli spinor states, the Hamiltonian containing only the scalar potential is diagonalized in the LAPW basis: this is the first-variational step. The scalar states thus obtained are then used as a basis to set up a second-variational Hamiltonian with spinor degrees of freedom[56]. This is more efficient than simply using spinor LAPW functions, but care must be taken to ensure that there is a sufficient number of first-variational eigenstates for convergence of the second-variational problem. For example, 394 states per  $\mathbf{k}$ -point were used for the pnictides to ensure convergence of the second variational step. We use a  $\mathbf{k}$ -point set of  $20 \times 20 \times 10$  for pinictides and  $20 \times 20 \times 20$  for the rest of the materials. A smearing width of 0.027eV was used.

## Separate scaling and removal of source term

It is also interesting to investigate separately the effect of making the functional source-free and scaling it. We found that the purely source-free LSDA and GGA functionals lead to highly under estimated moments (see Table III). This is due to suppression of the  $z$ -projected moment. The magnetization density obtained by purely source-free LSDA and GGA is also highly non-collinear (i.e.  $x$  and  $y$  projected moments are as significant as  $M_z$ ). The scaling alone of the LSDA/GGA has, as expected, rather trivial effect of increasing the moment universally since the whole  $\mathbf{m}(\mathbf{r})$  is uniformly scaled. One could envisage using the scaling parameter so as to reproduce experimental moment for the materials. This, however, has the disadvantage that the scaling parameter is then highly material-dependent. The combination of the two things (scaling and source-free) leads to good agreement with experiments for a wide set of materials and most importantly the scaling factor depends only on the choice of original functional.

---

\* Electronic address: sharma@mpi-halle.mpg.de

[1] P. Hohenberg and W. Kohn, Phys. Rev. **136**, B864 (1964).

TABLE III: Magnetic moment (in  $\mu_B$ ) per Fe atom for pnictides and per magnetic atom for the rest of the materials. LSDA<sub>s</sub>/GGA<sub>s</sub> moments are calculated by enhancing the LSDA, GGA magnetization density by 1.12 and 1.14 respectively. LSDA/GGA no source results are obtained by making LSDA/GGA source free (i.e. without any scaling)

Material	Expt	LSDA <sub>s</sub>	LSDA no source	GGA <sub>s</sub>	GGA no source
LaFeAsO	0.63	2.11	0.07	2.42	0.06
CeFeAsO	0.8	2.12	0.02	2.37	0.01
PrFeAsO	0.5	2.30	0.15	2.40	0.12
NdFeAsO	0.54	2.20	0.32	2.43	0.30
CaFe <sub>2</sub> As <sub>2</sub>	0.8	2.20	0.07	2.46	0.06
SrFe <sub>2</sub> As <sub>2</sub>	0.94	2.24	0.06	2.50	0.04
BaFe <sub>2</sub> As <sub>2</sub>	0.87	2.40	0.06	2.51	0.05
FeTe	2.25	2.60	0.88	2.67	0.95
bcc-Fe	2.2	2.62	1.91	2.66	1.90
hcp-Co	1.7	1.82	1.28	1.87	1.35
Ni	0.65	0.71	0.53	0.69	0.57
Ni <sub>3</sub> Al	0.077	0.26	0.01	0.29	0.06
ZrZn <sub>2</sub>	0.085	0.27	0.17	0.36	0.20

- [2] W. Kohn and L. J. Sham, Phys. Rev. **140**, A1133 (1965).
- [3] J. P. Perdew and Y. Wang, Phys. Rev. B **45**, 13244 (1992).
- [4] J. P. Perdew, K. Burke, and M. Ernzerhof, Phys. Rev. Lett. **78**, 1396 (1997).
- [5] P. Dai, Rev. Mod. Phys. **87**, 855 (2015).
- [6] I. I. Mazin, Nature **464**, 183 (2010).
- [7] A. A. Kordyuk, Low Temperature Physics **38**, 888 (2012).
- [8] P. Dai, J. Hu, and E. Dagotto, Nat Phys **8**, 709 (2012).
- [9] T. Yildirim, Phys. Rev. Lett. **101**, 057010 (2008).
- [10] D. J. Singh and M.-H. Du, Phys. Rev. Lett. **100**, 237003 (2008).
- [11] F. Ma, Z.-Y. Lu, and T. Xiang, Phys. Rev. B **78**, 224517 (2008).

- [12] S. Sharma, S. Shallcross, J. K. Dewhurst, A. Sanna, C. Bersier, S. Massidda, and E. K. U. Gross, Phys. Rev. B **80**, 184502 (2009).
- [13] L. Ortenzi, H. Gretarsson, S. Kasahara, Y. Matsuda, T. Shibauchi, K. D. Finkelstein, W. Wu, S. R. Julian, Y.-J. Kim, I. I. Mazin, et al., Phys. Rev. Lett. **114**, 047001 (2015).
- [14] F. Essenberger, P. Buczek, A. Ernst, L. Sandratskii, and E. K. U. Gross, Phys. Rev. B **86**, 060412 (2012).
- [15] I. I. Mazin, D. J. Singh, M. D. Johannes, and M. H. Du, Phys. Rev. Lett. **101**, 057003 (2008).
- [16] J. Lischner, T. Bazhiron, A. H. MacDonald, M. L. Cohen, and S. G. Louie, Phys. Rev. B **91**, 020502 (2015).
- [17] F. Essenberger, A. Sanna, P. Buczek, A. Ernst, L. Sandratskii, and E. K. U. Gross, Phys. Rev. B **94**, 014503 (2016).
- [18] U. von Barth and L. Hedin, Journal of Physics C: Solid State Physics **5**, 1629 (1972).
- [19] L. M. Sandratskii and P. G. Guletskii, Journal of Physics F: Metal Physics **16**, L43 (1986).
- [20] J. Kubler, K. H. Hock, J. Sticht, and A. R. Williams, Journal of Physics F: Metal Physics **18**, 469 (1988).
- [21] N. I. Gidopoulos, Phys. Rev. B **75**, 134408 (2007).
- [22] H. Eschrig, G. Seifert, and P. Ziesche, Solid State Communications **56**, 777 (1985).
- [23] K. Capelle and E. K. U. Gross, Phys. Rev. Lett. **78**, 1872 (1997).
- [24] X. Gonze, P. Ghosez, and R. W. Godby, Phys. Rev. Lett. **74**, 4035 (1995).
- [25] S. Sharma, J. K. Dewhurst, C. Ambrosch-Draxl, S. Kurth, N. Helbig, S. Pittalis, S. Shallcross, L. Nordström, and E. K. U. Gross, Phys. Rev. Lett. **98**, 196405 (2007).
- [26] L. Ortenzi, I. I. Mazin, P. Blaha, and L. Boeri, Phys. Rev. B **86**, 064437 (2012).
- [27] URL <http://elk.sourceforge.net>.
- [28] A. S. Sefat, A. Huq, M. A. McGuire, R. Jin, B. C. Sales, D. Mandrus, L. M. D. Cranswick, P. W. Stephens, and K. H. Stone, Phys. Rev. B **78**, 104505 (2008).
- [29] N. Qureshi, Y. Drees, J. Werner, S. Wurmehl, C. Hess, R. Klingeler, B. Büchner, M. T. Fernández-Díaz, and M. Braden, Phys. Rev. B **82**, 184521 (2010).
- [30] The PBE optimised lattice parameters for LaOFeAs are  $a = 5.693\text{\AA}$ ,  $b = 5.761\text{\AA}$ ,  $c = 8.705\text{\AA}$ ,  $Z_{\text{As}} = 0.64608$  and for BaFe<sub>2</sub>As<sub>2</sub> are  $a = 5.61\text{\AA}$ ,  $b = 5.707\text{\AA}$ ,  $c = 12.872\text{\AA}$ ,  $Z_{\text{As}} = 0.6497$ .
- [31] J. Zhao, Q. Huang, C. de la Cruz, S. Li, J. W. Lynn, Y. Chen, M. A. Green, G. F. Chen, G. Li, Z. Li, et al., Nat Mater **7**, 953 (2008).

- [32] Q. Zhang, W. Tian, H. Li, J.-W. Kim, J. Yan, R. W. McCallum, T. A. Lograsso, J. L. Zarestky, S. L. Bud'ko, R. J. McQueeney, et al., Phys. Rev. B **88**, 174517 (2013).
- [33] J. Zhao, Q. Huang, C. de la Cruz, J. W. Lynn, M. D. Lumsden, Z. A. Ren, J. Yang, X. Shen, X. Dong, Z. Zhao, et al., Phys. Rev. B **78**, 132504 (2008).
- [34] S. A. J. Kimber, D. N. Argyriou, F. Yokaichiya, K. Habicht, S. Gerischer, T. Hansen, T. Chatterji, R. Klingeler, C. Hess, G. Behr, et al., Phys. Rev. B **78**, 140503 (2008).
- [35] Y. Qiu, W. Bao, Q. Huang, T. Yildirim, J. M. Simmons, M. A. Green, J. W. Lynn, Y. C. Gasparovic, J. Li, T. Wu, et al., Phys. Rev. Lett. **101**, 257002 (2008).
- [36] W. Tian, W. Ratcliff, M. G. Kim, J.-Q. Yan, P. A. Kienzle, Q. Huang, B. Jensen, K. W. Dennis, R. W. McCallum, T. A. Lograsso, et al., Phys. Rev. B **82**, 060514 (2010).
- [37] A. Kreyssig, M. A. Green, Y. Lee, G. D. Samolyuk, P. Zajdel, J. W. Lynn, S. L. Bud'ko, M. S. Torikachvili, N. Ni, S. Nandi, et al., Phys. Rev. B **78**, 184517 (2008).
- [38] A. I. Goldman, D. N. Argyriou, B. Ouladdiaf, T. Chatterji, A. Kreyssig, S. Nandi, N. Ni, S. L. Bud'ko, P. C. Canfield, and R. J. McQueeney, Phys. Rev. B **78**, 100506 (2008).
- [39] M. Tegel, M. Rotter, V. Wei, F. M. Schappacher, R. Pttgen, and D. Johrendt, Journal of Physics: Condensed Matter **20**, 452201 (2008).
- [40] J. Zhao, W. Ratcliff, J. W. Lynn, G. F. Chen, J. L. Luo, N. L. Wang, J. Hu, and P. Dai, Phys. Rev. B **78**, 140504 (2008).
- [41] R. Mittal, S. K. Mishra, S. L. Chaplot, S. V. Ovsyannikov, E. Greenberg, D. M. Trots, L. Dubrovinsky, Y. Su, T. Brueckel, S. Matsuishi, et al., Phys. Rev. B **83**, 054503 (2011).
- [42] Q. Huang, Y. Qiu, W. Bao, M. A. Green, J. W. Lynn, Y. C. Gasparovic, T. Wu, G. Wu, and X. H. Chen, Phys. Rev. Lett. **101**, 257003 (2008).
- [43] F. Caglieris, F. Ricci, G. Lamura, A. Martinelli, A. Palenzona, I. Pallecchi, A. Sala, G. Profeta, and M. Putti, Science and Technology of Advanced Materials **13**, 054402 (2012).
- [44] S. Li, C. de la Cruz, Q. Huang, Y. Chen, J. W. Lynn, J. Hu, Y.-L. Huang, F.-C. Hsu, K.-W. Yeh, M.-K. Wu, et al., Phys. Rev. B **79**, 054503 (2009).
- [45] The value of  $U$  and  $J$  used with LSDA functional are  $U = 2.04\text{eV}$ ,  $J = 0.57\text{eV}$  for NdFeAsO,  $U = 3.27\text{eV}$ ,  $J = 0.67\text{eV}$  for PrFeAsO. The values used in combination of GGA are  $U = 4.7\text{eV}$ ,  $J = 1.4\text{eV}$  for NdFeAsO,  $U = 2.04\text{eV}$ ,  $J = 1.15\text{eV}$  for PrFeAsO.
- [46] Moment for Pr atom: LSDA<sub>SF</sub> =  $1.67\mu_B$ , GGA<sub>SF</sub> =  $1.8\mu_B$  and for Nd atom: LSDA<sub>SF</sub> =  $2.9\mu_B$ , GGA<sub>SF</sub> =  $2.9\mu_B$ .

- [47] A. I. Liechtenstein, V. I. Anisimov, and J. Zaanen, Phys. Rev. B **52**, R5467 (1995).
- [48] C. de la Cruz, Q. Huang, J. W. Lynn, J. Li, W. Ratcliff, J. L. Zarestky, H. A. Mook, G. F. Chen, J. L. Luo, N. L. Wang, et al., Nature **453**, 899 (2008).
- [49] H.-F. Li, W. Tian, J.-Q. Yan, J. L. Zarestky, R. W. McCallum, T. A. Lograsso, and D. Vaknin, Phys. Rev. B **82**, 064409 (2010).
- [50] A. Aguayo, I. I. Mazin, and D. J. Singh, Phys. Rev. Lett. **92**, 147201 (2004).
- [51] D. J. Singh and I. I. Mazin, Phys. Rev. Lett. **88**, 187004 (2002).
- [52] Z. P. Yin, S. Lebègue, M. J. Han, B. P. Neal, S. Y. Savrasov, and W. E. Pickett, Phys. Rev. Lett. **101**, 047001 (2008).
- [53] T. Yildirim, Phys. Rev. Lett. **102**, 037003 (2009).
- [54] N. Colonna, G. Profeta, A. Continenza, and S. Massidda, Phys. Rev. B **83**, 094529 (2011).
- [55] I. I. Mazin, M. D. Johannes, L. Boeri, K. Koepernik, and D. J. Singh, Phys. Rev. B **78**, 085104 (2008).
- [56] D. J. Singh and L. Nordström, Planewaves Pseudopotentials and the LAPW Method, pringer, New York (2006).